



Research Paper

## Effects of Magnetic Fields on Diffusion Flames

Diego Gonzalez, Sumathi Swaminathan, and Tryfon T. Charalampopoulos\*

Combustion and Laser Diagnostics Laboratory

Department of Mechanical Engineering, Louisiana State University Baton Rouge, LA 70803, USA

Corresponding author: Diego Gonzalez

**ABSTRACT:** Magnetic field effects in combustion processes is an area of study that has previously been overlooked. The influence of magnetic fields on flames has only recently been explored and is of interest both from a scientific and a practical standpoint. This study provides numerical and experimental evidence that combustion can be affected with the use of suitable magnetic fields. Four different magnetic configurations were tested using Finite Element Methods to obtain the force field profile on paramagnetic oxygen. Numerical simulations showed that high magnetic field gradients at high magnetic strengths, such as those exerted by spherical permanent magnets, are most suitable to enhance oxygen entrainment into a reaction zone. The effects of gradient magnetic fields were also tested experimentally in a diffusion flame and results showed a decrease in soot agglomeration for decreasing gradient fields. The size of the agglomerated particles was estimated using image-processing techniques and a 69.4% reduction in agglomerate area was calculated. The flame structure of a diffusion flame was analyzed using digital imagery and a redistribution of the velocity profile was visualized with the application of a magnetic field.

Received 20 Oct. , 2019; Accepted 03 Nov. , 2019 © The author(s) 2019.

Published with open access at [www.questjournals.org](http://www.questjournals.org).

### I. INTRODUCTION

Since the time of Faraday, there have been few studies on the effects of magnetic fields on flames. Faraday, in his original investigation, realized that the application of certain magnetic field configurations to a burning candle resulted in an equatorial elongation of the combustion zone [1]. More recently, researchers have confirmed what Faraday observed over a century earlier by demonstrating that flames bent to escape magnetic fields of higher intensities. Ueno and Harada [2] began experimenting with diffusion flames. After confirming Faraday's results, the authors tested gas flows without undergoing a combustion process. All gases analyzed were blocked or modified by the gradient magnetic fields. Oxygen concentration was continuously measured and was increased in all of the different gas flows. They concluded that oxygen is aligned so as to form a "wall of oxygen". They used different velocity flows to test the strength of the "wall of oxygen". This air curtain extended between magnetic poles in areas where both magnetic fields and gradients were high enough. It was observed by the authors that the wall was strong enough to press back on flames and gas flow. They attributed these results to the paramagnetic nature of oxygen and to the forces that were produced on air by the introduction of a magnetic field. Later studies [3-8] contradicted the "wall of oxygen" theory by instead proving the presence of an oxygen convective flow through the gradient magnetic field.

Wakayama and Masaaki [3] conducted magnetic experiments on methane diffusion flames. They observed the effects of inhomogeneous magnetic fields by both measuring temperature differences and observing variations in flame shape, color and size. Under a homogeneous magnetic field, no change was observed. On the other hand, for a decreasing magnetic gradient in the direction of the flow, the flame became shorter, sharper and more brilliant. The velocity of air into the flame front under decreasing magnetic field was calculated using energy conservation and was about three orders larger than the rate of diffusion. Several researchers confirmed these results in similar experiments [4-6]. Ruan [7] used digital particle velocimetry (DIPV) techniques to measure the velocity distribution of gas flows around diffusion flames under magnetic fields. The author quantitatively verified the existence of flows of oxygen induced by gradient magnetic fields. In all of these studies, oxygen was shown to be attracted towards regions of stronger magnetic field, while nitrogen and other combustion products were repelled towards a weaker field. This phenomenon was mainly attributed to the difference in magnetic susceptibility of gas species. Oxygen, being paramagnetic in nature, has

a positive magnetic susceptibility while the rest of the combustion products are diamagnetic and have negative magnetic susceptibility.

Numerical simulations of diffusion flames with and without magnetic field were performed by Kinoshita et al [8]. Axis-symmetric laminar jet diffusion flames under normal and microgravity environments were studied. The fundamental equations considered were conservation of mass, axial momentum, radial momentum, species and energy. Velocity vectors and temperature contours were plotted for gradient magnetic fields under microgravity and normal gravity conditions. Again, it was observed that convection around the diffusion flame is induced by magnetic forces. The flow under microgravity with a gradient magnetic field is similar to the one under normal gravity without magnetic fields. This study again confirms that a magnetic flow of oxygen promotes combustion in diffusion flames.

The present study focuses on identifying optimum magnetic configurations to augment oxygen flow into the reaction zone of a diffusion flame. The Finite Element Method Magnetics software package [9] was used to simulate the magnetic fields exerted by readily obtainable magnet configurations. Plots were then used to obtain the regions of highest magnetic force on a gas species. Propane diffusion flames under an applied magnetic field were experimentally tested in regions of high magnetic forces on paramagnetic oxygen. Soot samples were extracted from the flame and digitally processed to estimate the amount of agglomerate reduction obtained with the use of magnetic fields. In addition, digital flame images were also used to visualize the changes in flame structure under the application of a magnetic field.

## II. METHODOLOGY

This study is divided into two different parts: numerical and experimental. The first part focuses on finding the best type of magnetic field configuration that exerts the highest volumetric force on paramagnetic oxygen. The experimental part describes the effects of magnetic fields on soot emissions as well as flame structure.

### (A) NUMERICAL STUDY

The numerical study focuses on analyzing different types of magnetic fields to identify a magnetic field configuration that can positively affect combustion characteristics. Main focus is given to the effects of the fields on paramagnetic oxygen. Finite Element Method Magnetics are used to find the flux density profile along the central axis of four different types of magnetic configurations. For comparison purposes, the gap in between magnetic surfaces was kept constant (3 cm air gap) for all the simulations. Convergence was checked in the numerical analysis by reducing the mesh size until no perceivable changes in the results were obtained. Also, the simulation results were validated by experimental measurements using a Gauss meter (Lakeshore 420). The simulations were performed in the following magnetic configurations:

1. Experimental Electromagnet: Electromagnet configuration used in previous combustion studies [6, 8] and also used in the experimental part of this study.
2. Gradient Solenoid: Copper solenoid modified to induce a gradient magnetic field by coiling the wire at a slope of 30° with respect to the vertical (Figure 1).
3. Circular Permanent Magnets: Common Neodymium permanent magnets with a circular, 5 cm diameter cross-section and a horizontal magnetic alignment (Figure 2).
4. Rectangular Permanent Magnets: Common Neodymium permanent magnets with a rectangular cross-section (5cm X 4 cm). To form a gradient field, the magnets were oriented at 45° with respect to the vertical.

The simulated magnetic flux densities were used to generate analytical expressions for the profiles. The magnetic force on gas species is governed by equation (1),

$$F_i = \frac{1}{2} \frac{\chi_i}{m_o} \bar{B} \frac{d\bar{B}}{dz} \quad (1)$$

where  $\chi_i$  is the magnetic susceptibility of species  $i$ ,  $\mu_o$  is the permeability of free space,  $\bar{B}$  is the magnetic flux density and  $d\bar{B}/dz$  is the magnetic flux gradient. As it may be seen from equation (1), the magnetic force on a gas species is proportional to both the magnetic flux density and the magnetic flux gradient. Matlab was used to calculate the force profile on paramagnetic oxygen as a function of vertical position for each of the magnetic configurations.

### (B) EXPERIMENTAL STUDY

The experimental system consisted of a diffusion type propane/air flame centered on a stainless steel burner tube (1/4 inch in diameter). Regulated fuel was supplied to the burner. The electromagnet used was set-up by using a permanent magnet with a cast Iron core and magnetic wire winding connected to a DC power supply. The magnetic field flux in the central axis was measured with an uncertainty of 2% due to the difficulty

of the placement of the probe within the air-gap. The study was carried out in two flow regimes. Firstly, in the non-sooting regime corresponding to flow rates ranging from 17 cc/min-105 cc/min were studied for the influence on the flame height. In the sooting regime, soot particles produced in the flame were collected through a thermophoretic sampling system and deposited on to a 200-mesh copper grid coated with carbon film that is stable under electron beam exposure for subsequent transmission electron microscopy (TEM). Matlab was used for digital processing of the soot images. Finally, a platinum versus platinum-10% rhodium (S-Type) thermocouple was used to measure the temperature at various axial locations of the flame utilizing a vertical translation mechanism.

### III. RESULTS AND DISCUSSION

#### (A) NUMERICAL STUDY

The magnetic flux density profile around the cross-section of the different magnetic configurations was found with a convergence criteria of  $10^{-8}$ . Figures 2 and 3 show a representation of the results obtained from the simulations. To validate the numerical results, experimental measurements were taken in the air-gap region of the electromagnet (Figure 4). In comparison, the results exhibit the same trends although the experimental maximum value is 0.09 T lower than the numerical. These differences may be attributed to geometrical discrepancies between the model and the electromagnet, material differences (pure iron versus cast iron) and a 2% experimental uncertainty in the measurements due to the difficulties in the precise placement of the probe.

Plots of magnetic flux density with respect to vertical position were obtained for the electromagnet, the circular permanent magnets and the rectangular permanent magnet configurations. An example of the magnetic profile plots that were obtained is presented in Figure 5. Since the solenoid is on an axis-symmetric plot, the magnetic gradients occur on the radial direction. Plots for the solenoid were obtained at the center of solenoid in the radial direction. The appropriate polynomial curve fit was found for all configurations by using the equation that had a Pearson's coefficient of determination [13] of around  $\sim 0.999$ .

The curve-fitted polynomials were used to calculate the magnetic flux gradients ( $d\vec{B}/dz$ ). Using equation (1) and the magnetic susceptibility data from [14], the magnetic force on oxygen as a function of position for each of the configurations was plotted (Figure 6).

For all cases except the solenoid, the force on oxygen changes direction from positive to negative. The plot also shows that the circular permanent magnets exert the maximum force mainly due to the large gradients. The rectangular magnets have a larger maximum force in the positive than in the negative direction. The electromagnets are third on the maximum force followed by the solenoid, which exerts rather negligible forces on oxygen. For comparison purposes, the magnitude and direction of the maximum force exerted by each of the magnetic configurations is shown in Table 1.

#### (B) EXPERIMENTAL STUDY

##### i. Effects on flame height and oxygen mole fractions

A comparison of the flame height with and without the magnetic field is shown in Table 2. When the flame is subjected to a vertically decreasing field gradient, the flame height decreased for the entire range of flow rates studied. For the same flow rates, the flame was subjected to an increasing field gradient and it was found that the results were consistent with previous findings [3-4, 7], i.e. the flame heights increased for all the flow rates due to the reduction of oxygen entrainment in the reaction zone. A visual examination of the flame structure/shape suggested that the flame was being turned away from the magnetic field of higher intensities, for this field orientation.

To estimate the amount of oxygen concentration increased with the use of magnetic fields, a widely used expression to predict laminar jet flame lengths for circular burner ports derived by Roper [15] may be used. The expression applies to flames regardless of whether or not buoyancy is important in the reaction and is applicable for fuel jets emerging into a quiescent oxidizer or a co-flowing stream. Given that magnetic forces are similar to buoyant forces (both act on a volumetric basis) it may be assumed that the expression developed by Roper applies for laminar diffusion flames under the application of a magnetic field. Roper's expression for the flame length in a circular port is as follows:

$$L_f = 1330 \frac{Q_f (T_\infty / T_f)}{\ln(1 + 1/S)} \quad (2)$$

where  $Q_f$  is the volumetric flow rate of fuel from the nozzle ( $m^3/sec$ ),  $T_\infty$  is the ambient oxidizer temperature (K),  $T_f$  is the mean flame temperature at the burner exit (K), and  $S$  is the molar-stoichiometric oxidizer-fuel ratio. For a generic hydrocarbon,  $C_xH_y$ , the stoichiometric ratio can be expressed as

$$S = \frac{x + y/4}{C_{O_2}} \quad (3)$$

where  $C_{O_2}$  is the mole fraction of oxygen in air.

Substituting Equation (3) into (2) and solving for the mole fraction of oxygen in air results in:

$$C_{O_2} = \left(x + \frac{y}{4}\right) \exp\left[\frac{Q_f(T_f/T_f) - 1330}{\ln(1 + 1/S)}\right] \quad (4)$$

From the experimental data for flame length and flame temperature for the propane diffusion flame, the changes in mole fraction of oxygen for the case of an applied magnetic field can be compared to the no magnetic field case. Flame temperature data was taken for jet velocities of 0.9 cm/sec and 2.6 cm/sec. For these same speeds, flame lengths were measured for the cases of applied magnetic field (magnetic strength of 0.27 Tesla at a gradient of -24 T/m) and no applied magnetic field. By averaging the temperature measurements and using the measured flame lengths, the increase in oxygen concentration was found and summarized in the Table 3.

For the case of 0.9 cm/sec velocity, the increase in oxygen concentration was of 20.3% while the case of 2.6 cm/sec jet velocity only produced an increase of 2.68%. The lower velocity case has a larger increase in oxygen entrainment since the momentum is lower in the axial direction. As velocity increases in the jet flow, the momentum force becomes dominant and the effects of the magnetic force on paramagnetic oxygen are reduced. The domain of interaction in which a flame may be affected by magnetic fields of moderate flames may be calculated by comparing the momentum forces of the fuel jet to the magnetic forces required to impact this jet. The equation for the volumetric momentum force in a jet can be written as

$$F_{mom} = \frac{\int \rho v_f^2 dA}{\int l dA} \quad (5)$$

where  $\rho$  is the density,  $v_f$  is the velocity of the fuel gas at the jet exit,  $dA$  is the differential area of the jet and  $l$  is the characteristic length. The momentum force can be calculated for a range of velocities to identify the flow velocities where magnetic fields of moderate strengths can cause an effect on oxygen. The magnetic force from equation (1) with a fixed gradient of 24 T/m and field intensities of up to 1.0 Tesla was used to calculate the magnetic force on the fuel gas. A comparison of the forces is seen in Figure 7 and as expected, the momentum force increases as the Reynolds number increases. The magnetic force takes a value of about 50 N/m<sup>3</sup> for field intensities of 1.0 Tesla. By comparing the magnitudes of the forces it can be seen that moderate magnetic field strengths (0.2-0.8 T) may be used to affect low Reynolds number flows (Re in the range of 10-100). This explains the decreased effect on oxygen concentration at the higher velocity flow.

In a similar fashion, the magnetic forces may be compared to the buoyancy forces with the equation for buoyancy acting on the flame,

$$F_b = \left(\rho_f(h) - \rho_\infty\right)g \quad (6)$$

where  $\rho_f(h)$  is the density of the flame as a function of height,  $\rho_\infty$  the density of the ambient gas and  $g$  is the gravity constant. A comparison for the forces acting on oxygen at a fixed Reynolds number of 15 was performed. For this flow velocity, Figure 8 shows that the buoyancy forces are dominant since these are 10<sup>4</sup> orders of magnitude larger than the momentum forces. Moreover, Figure 9 demonstrates that the magnetic forces are of similar magnitude as the buoyancy forces, thus having a clear effect on the system when they act on the same direction as the buoyancy forces.

## ii. Effects on soot emissions

The effect of the gradient magnetic field on sooting flames was also investigated. Morphological characterization of the soot collected in these flames with and without the field was carried out as a function of the height above the burner surface along the flame axis. Towards this end, a stable flame corresponding to a flow rate of 145 cc/min was established and was chosen as the test case for all the soot morphological measurements both within the flame and the flame tip [6]. The flame borne particles were thermophoretically sampled on to copper coated carbon grids and analyzed using a transmission electron microscope (TEM). The TEM micrographs sampled at the flame tip are shown in Figure 10. The soot particles are agglomerated into random clusters as visualized from the images. The images indicate a decrease in the amount of soot particle aggregates as well as size, for the case of a vertically decreasing magnetic field as compared to the case without the application of a magnetic field. To quantify this reduction, the Matlab image processing toolbox was used to analyze the photographs.

Images of soot agglomeration can be used to infer the size distribution of individual particles without explicitly detecting each object first. Granulometry, in Matlab was used to estimate the intensity surface area distribution of particles as a function of size. Granulometry likens image objects to stones whose sizes can be determined by sifting them through screens of increasing size and collecting what remains after each pass. Objects are sifted by opening the image with a structuring element of increasing size and counting the remaining intensity surface area (summation of pixel values in the image) after each opening. The intensity surface area distribution was determined from the TEM images and plotted in Figures 11.

A significant drop in intensity surface area between two consecutive openings indicates that the image contains objects of comparable size to the smaller opening. This is equivalent to the first derivative of the intensity surface area array, which contains the size distribution of the particles in the image. The derivative of the size distribution of particles can then be plotted as shown in Figure 12. The minima in the plots determine the radii of the particles that are most occurring in the image. The more negative the minimum point, the higher the particles' cumulative intensity at that radius.

It can be noticed that the minima occurs at a radius of 6 pixels for the case of no applied magnetic field while it occurs at a radius of 5 pixels for an applied magnetic field. Being that in these images 1 micrometer is equal to 220 pixels, the radius of the most occurring particles are 27.3 nanometers and 22.7 nanometers for the case of no applied magnetic field and applied magnetic field, respectively. These values are consistent with the ones in the literature, which suggest that agglomerates are formed from spherical particles measuring approximately 10-40 nm such as the results reported in [16, 17], among others. This result suggests that a decrease of 16.85% in primary particle size occurs in the presence of magnetic field.

Although the size of the particles did not change significantly, it was clear from the images that the quantity of the agglomerates certainly decreased. In order to quantify the decrease of particle agglomeration, another image processing technique was used. The method used involved enhancing the image to correct for non-uniform illumination and then use the enhanced image to identify individual particle agglomerates. This first required that the background of the image be removed and then the image be converted to binary. This allowed the labeling of connected components in the binary images. Each distinct object was labeled with an individual integer value and was easily visualized in a color-indexed image as in Figure 13. Once the regions in the image were labeled, Matlab was used to measure the area of the objects. Table 4 summarizes the properties found from the two images analyzed. A closer examination of these results reveals the following: Although the number of agglomerates was larger for the gradient magnetic field, the maximum area of these agglomerates was about 69.4% smaller than the case of no magnetic field. Also, the mean area for the agglomerates decreased by 68.9% when a magnetic field is used. These results showed that even though the size of the particles formed in the soot based on the present data analysis changed by approximately 17%, the formation of random of agglomerates was significantly decreased with the use of magnetic fields. This suggests that the agglomerated particles are oxidized further in the flame tip, due to the augmentation of oxygen entrainment by paramagnetic attraction in higher magnetic field gradients.

### **iii. Effects on flame structure**

For analysis of flame structure under an applied magnetic field, another experiment on a propane diffusion flame was performed ad-hoc. Two Neodymium grade 40, 1.5 inch diameter magnetic spheres were used to apply a magnetic field on the diffusion flame. The same burner described in the methodology section was used and the flow rate of propane was measured using a Singer American dry test flow meter model 115 and kept constant to provide a jet exit velocity of 2.5 cm/sec. Digital images were acquired using a digital camera for the case of applied magnetic field versus the case of no magnetic field. The magnets were aligned in a way that the center of the spheres was in-line with the exit nozzle of the burner. The burner central axis was placed in the center of the air gap, which was kept at 1 inch. This placed the combustion reaction zone approximately 1 mm above the center of the field under a vertically decreasing magnetic gradient, which is the prescribed condition for combustion enhancement. This configuration resulted in a maximum magnetic field strength of 0.37 Tesla, which was measured with a Gauss meter using a transverse probe.

Flame images were taken at a constant flow rate for the two different cases analyzed. The flow rate was chosen because the size of the flame at this preset speed allowed ease of visualization of the changing flame structure. The digital images were imported into Matlab, the background in the images was removed and the flames were segmented into three different colors: yellow, blue and white using a K-means clustering statistical analysis. The yellow color was the area of focus since it provides an accurate representation of the flame sheet structure. The digitally enhanced images are shown in Figure 14.

Changes in the flame structure that are not visually clear in the unedited images can be clearly seen after color segmentation. It can be seen from the images that the application of the magnetic field on the diffusion flame produces a shorter narrower flame due to the applied pressure of paramagnetic oxygen. This confirms observations seen by previous researchers [2-6]. An interesting feature that can be visualized is the

elimination of the arc formed near the exit of the flame. The arc is formed in the no applied magnetic field case is due to the parabolic velocity distribution of the fuel at the jet exit. The elimination of this arc suggests that the downward magnetic convection of oxygen slows down the fuel velocity, thus changing the shape of the velocity distribution.

#### IV. CONCLUSIONS

The effects of different magnetic fields on combustion characteristics have been explored. Numerical and experimental studies were carried out. The specific findings for each part of the study are as follows:

**a.** It was determined that magnets with high magnetic flux gradients at high magnetic strengths are more suitable to affect oxygen flow in a combustion process. In particular, circular permanent magnets with a horizontal magnetic alignment exerted the highest force due to the gradients that can be formed by surface curvature.

**b.** The effects of paramagnetic oxygen flow in a diffusion flame were tested experimentally in both decreasing and increasing magnetic gradients. It was shown that increasing oxygen flow with the use of magnetic gradients altered the flame structure and shape of a diffusion flame. Oxygen concentration was estimated to increase significantly in the diffusion flame for low Reynolds number flows.

**c.** A comparison of momentum, buoyancy and magnetic forces was performed and it was demonstrated that magnetic forces of moderate strength might be used to affect flames of Reynolds number in the range of 10-100.

**d.** It was shown that soot agglomeration is decreased with the use of decreasing gradient magnetic fields. This was attributed to enhanced soot oxidation due to the promotion of oxygen entrainment in the flames. The present results suggest that soot emission reductions are possible using suitably applied magnetic field configurations in the flame systems studied.

**e.** It is important to note that to enhance combustion characteristics of diffusion flames, the direction of the magnetic force on paramagnetic oxygen has to oppose the direction of the fuel flow so as to act as a buoyancy force that attracts oxygen towards the reaction zone.

**f.** The magnetic field applied to the diffusion flame confirmed results seen by previous researchers, showing a decrease in flame size. Digitally enhanced imagery showed that applying a magnetic field to the flame redistributes the parabolic velocity distribution of the fuel jet. This is attributed to the downward force of paramagnetic oxygen, which opposes the direction of fuel flow. By reducing the jet velocity, the fuel and oxidizer have more time to mix and more complete combustion can be achieved, and

**g.** Future work of magnetic field effects on combustion should focus on developing magnetic configurations that can provide for higher forces on paramagnetic oxygen. Complex magnet shapes and magnetic fields could be used to promote oxygen entrainment and mixing in combustion processes.

#### REFERENCES

- [1]. Faraday, M. On the Diamagnetic Conditions of Flames and Gases. The London, Edinburgh, and Dublin Philosophical Magazine and Journal of Science 31:401 (1847).
- [2]. Ueno, S., and Harada, K. Effects of magnetic fields on flames and gas flow. IEEE Transactions on Magnetics 23:2752 (1987).
- [3]. Wakayama, N. Magnetic promotion of combustion in diffusion flames. Combustion and Flame 93:207 (1993).
- [4]. Tanaka, H., Yoshida, K., Kimura, M., Shoji, H., Saima, A., and Higaki, M. Experimental Study of Diffusion and Stabilization on Diffusion Flames in Magnetic Field. Proceedings of the 2001 ASME Fluids Engineering Division Summer Meeting, New Orleans, LA, 2003, p. 91.
- [5]. Fujita, O., Ito, K., Chida, T., Nagai, S., and Takeshita, Y. Determination of magnetic field effects on a jet diffusion flame in a microgravity environment", Twenty-Seventh Symposium (International) on Combustion, The Combustion Institute, Pittsburgh, 1988, p. 2573.
- [6]. Swaminathan, Sumathi. Effects of Magnetic Field on Micro Flames. Master Thesis. Louisiana State University, Baton Rouge LA, 70803, 2005.
- [7]. Ruan, X. Experimental research on the promotion of combustion in diffusion flames by gradient magnetic field. Hangkong Xuebao/Acta Aeronautica et Astronautica Sinica 27:742 (2006).
- [8]. Kinoshita, S., Takagi, T., Kotera, H., and Wakayama, N. Numerical simulation of diffusion flames with and without magnetic field. IEEE Transactions on Applied Superconductivity 14:1685 (2004).
- [9]. Finite Element Method Magnetics <<http://femm.foster-miller.net/>>
- [10]. Rosenweig, R.E. Ferrohydrodynamics. Cambridge University Press, New York, 1985.
- [11]. Baker, John; Saito, Kozo. Magnetocombustion: A Thermodynamic Analysis. Journal of propulsion and power 16:263 (2000).
- [12]. Morley, C. GASEQ <http://www.arcl02.dsl.pipex.com>
- [13]. Rodgers, J. L. and Nicewander, W. A. Thirteen ways to look at the correlation coefficient. The American Statistician 42: 59-66 (1988).
- [14]. CRC Handbook of Chemistry and Physics. 87<sup>th</sup> Edition. CRC Press. Boca Raton, Florida, 1986.
- [15]. Roper, F. (1977). The Prediction of Laminar Jet Diffusion Flame Sizes: Part I. Theoretical Model. Combustion and Flame, 29:219-226.
- [16]. Chang, H. and Charalampopoulos, T. T. Determination of the wavelength dependence of refractive indices of flame soot. Proceedings of the Royal Society of London A 430, 577:591 (1990).
- [17]. Annamali, K., Puri, I. Combustion Science and Engineering. 1<sup>st</sup> Edition. CRC Press. Boca Raton, FL, 2007.
- [18].

TABLES

| Magnetic Configuration | Magnetic Force (N/m <sup>3</sup> ) |
|------------------------|------------------------------------|
| Electromagnet          | -1.59                              |
| Circular Permanent     | -3.36                              |
| Rectangular Permanent  | +2.34                              |
| Solenoid               | +0.074                             |

Table 1: Maximum magnetic force on oxygen for different configurations

| C <sub>3</sub> H <sub>8</sub> Velocity (cm/sec) | MEASURED FLAME LENGTH (cm) |   |   |
|---|----------------------------|---|---|
|   | No Field                   | B <sub>max</sub> =0.3 T Decreasing Gradient | B <sub>max</sub> =0.3 T Increasing Gradient |
| 5.2   | 5.64                       | 4.17  | 6.58  |
| 2.9   | 4.24                       | 3.68  | 4.7   |
| 2.6   | 2.62                       | 2.43  | 2.07  |
| 1.3   | 1.37                       | 1.07  | 1.65  |
| 1.2   | 1.22                       | 1.13  | 1.4   |
| 1.1   | 1.17                       | 0.9   | 1.22  |
| 0.9   | 1.02                       | 0.8   | 1.07  |

Table 2: Effects of magnetic fields on flame height

| Velocity (cm./sec) | Flame Length (cm) |                  | Average Flame Temp. (K) |                  | Oxygen Mole Fraction |                  |
|--------------------|-------------------|------------------|-------------------------|------------------|----------------------|------------------|
|                    | No Field          | Dec. Grad. Field | No Field                | Dec. Grad. Field | No Field             | Dec. Grad. Field |
| 0.9                | 1.02              | 0.80             | 1255                    | 1331             | 0.045                | 0.054            |
| 2.6                | 2.62              | 2.43             | 1214                    | 1275             | 0.052                | 0.053            |

Table 3: Oxygen mole fraction for decreasing gradient magnetic field versus case of no applied magnetic field at different velocities

| Property                   | No magnetic field                       | Dec. grad. magnetic field               |
|----------------------------|---|---|
| Number of agglomerates     | 84                                      | 141                                     |
| Max area                   | 0.261 μm <sup>2</sup>                   | 0.0796 μm <sup>2</sup>                  |
| Agglomerates with max area | 58                                      | 37                                      |
| Mean area                  | 9.56 X 10 <sup>-3</sup> μm <sup>2</sup> | 2.97 X 10 <sup>-3</sup> μm <sup>2</sup> |

Table 4: Soot agglomerate properties for no magnetic field and decreasing gradient magnetic field

LIST OF FIGURES

- Figure 1: Modified solenoid to form a gradient field (left), homogeneous field of a solenoid (right)
- Figure 2: Simulation results of magnetic flux around circular permanent magnets
- Figure 3: Simulation results of magnetic flux around experimental electromagnet
- Figure 4: Validation of numerical results by comparison to experimental measurements of magnetic flux density along the vertical central axis of the electromagnet
- Figure 5: Magnetic flux density for circular Neodymium magnets along the central axis
- Figure 6: Magnetic force on oxygen for different magnetic configurations
- Figure 7: Comparison of magnetic and momentum forces to establish a domain of interaction
- Figure 8: Comparison of forces- Ratio of buoyancy to momentum forces acting along a diffusion flame, Re=15
- Figure 9: Comparison of forces- Ratio of magnetic to buoyancy forces acting along a diffusion flame, Re=15
- Figure 10: Soot samples collected at flame tip for a case of (top) no magnetic field and (bottom) vertically decreasing magnetic field (B<sub>max</sub>=0.3 T)
- Figure 11: Surface Area Intensity plot for (top) no applied magnetic field and (bottom) decreasing gradient magnetic field
- Figure 12: Size distribution for (top) no applied magnetic field (bottom) decreasing gradient magnetic field
- Figure 13: Color indexed images of continuous objects in soot agglomerates
- Figure 14: Enhanced flame images for jet exit velocity of 2.5 cm/sec for no magnetic field (left) and spherical magnetic field on diffusion flame (right)

FIGURES

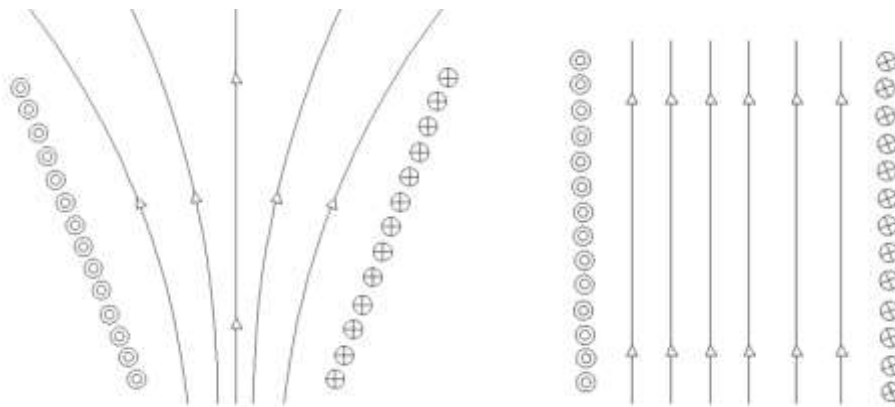


Figure 1: Modified solenoid to form a gradient field (left), homogeneous field of a solenoid (right)



Figure 2: Simulation results of magnetic flux around circular permanent magnets

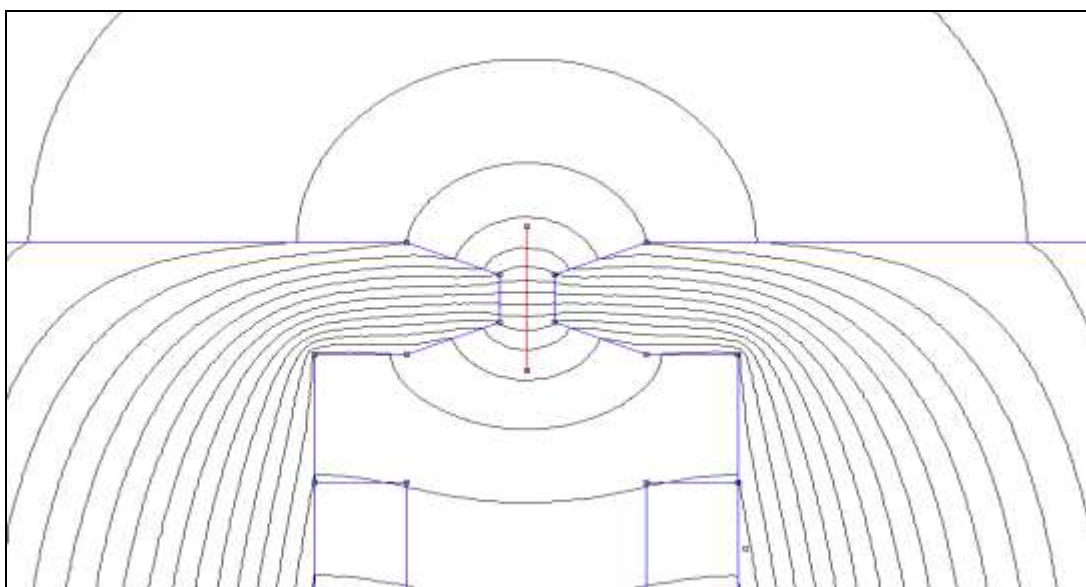
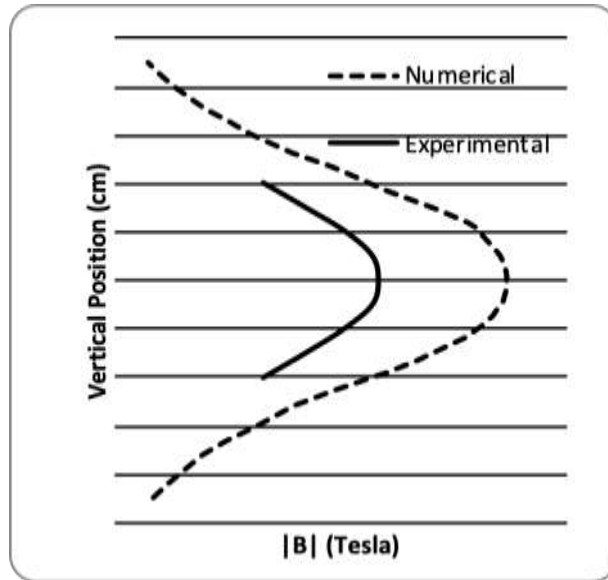
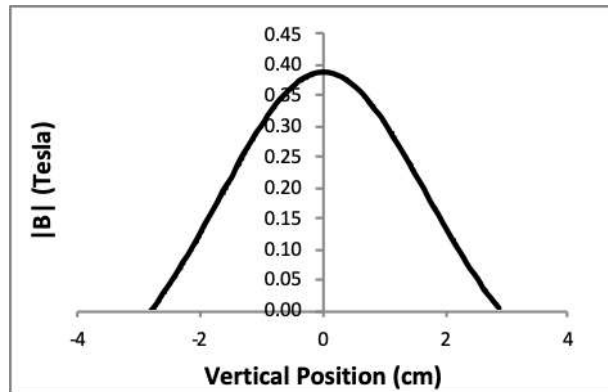


Figure 3: Simulation results of magnetic flux around experimental electromagnet



**Figure 4:** Validation of numerical results by comparison to experimental measurements of magnetic flux density along the vertical central axis of the electromagnet



**Figure 5:** Magnetic flux density for circular Neodymium magnets along the central axis

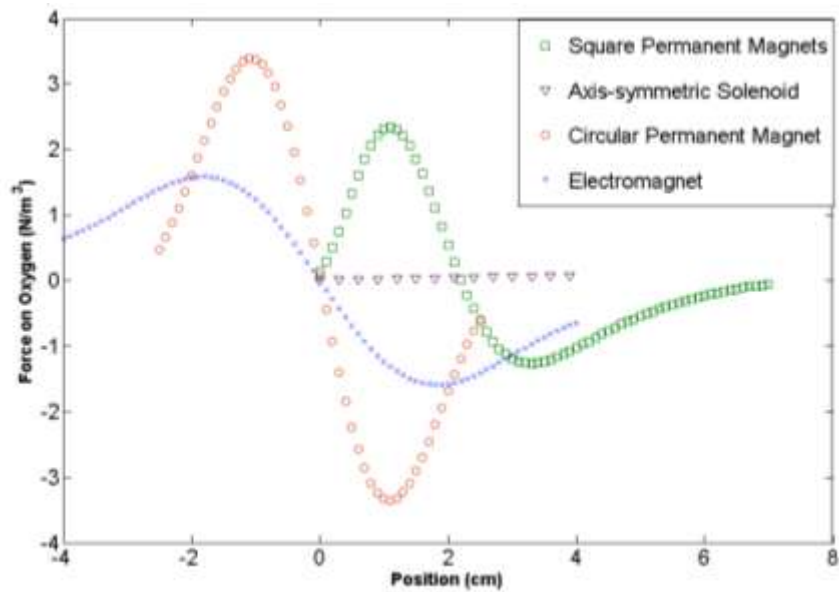


**Figure 6:** Magnetic force on oxygen for different magnetic configurations

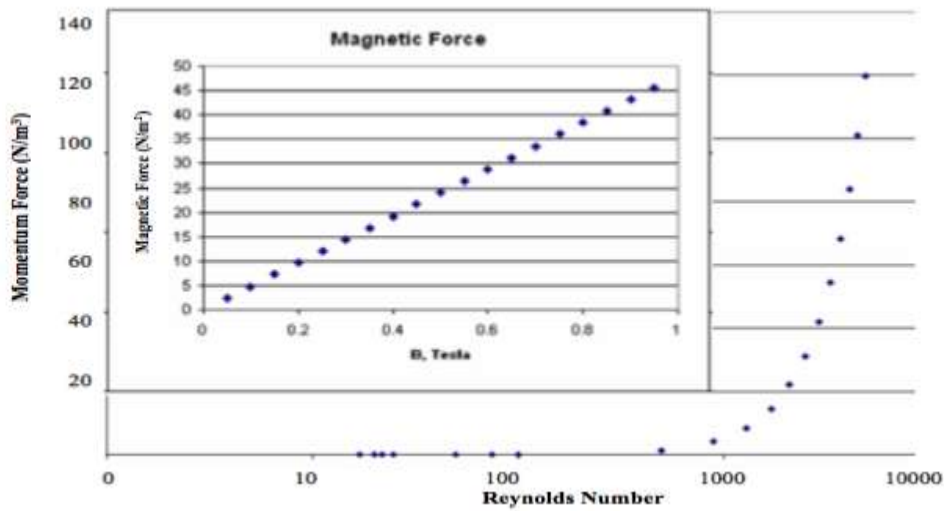


Figure 7: Comparison of magnetic and momentum forces to establish a domain of interaction

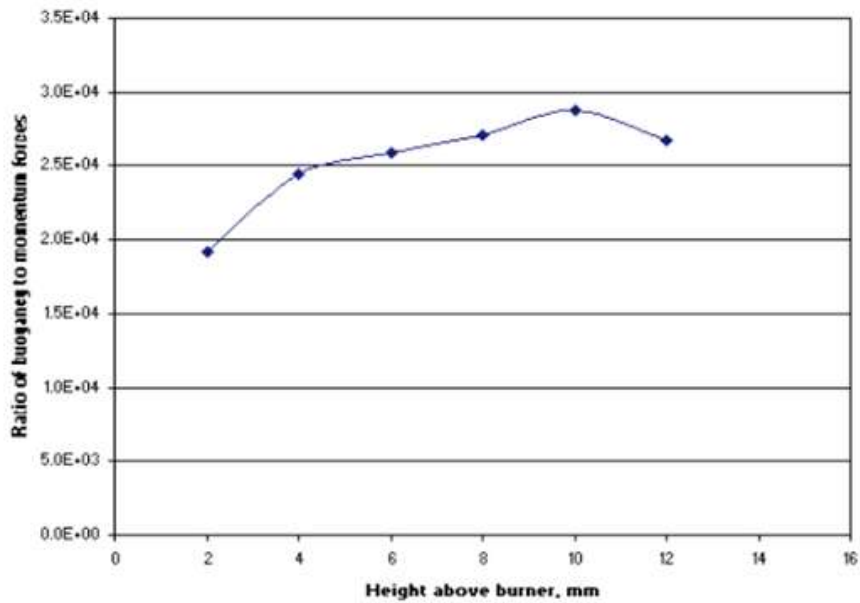


Figure 8: Comparison of forces- Ratio of buoyancy to momentum forces acting along a diffusion flame, Re=15

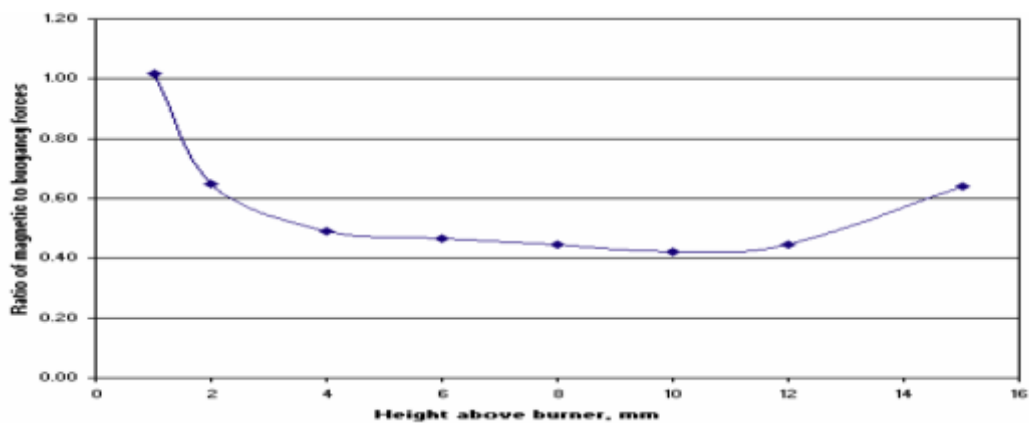
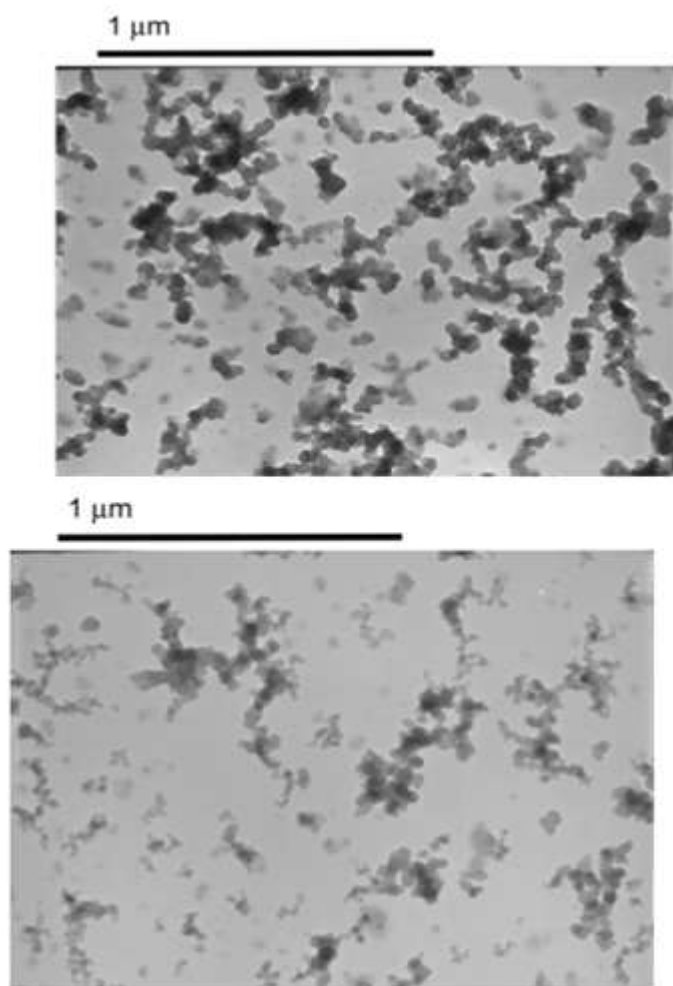
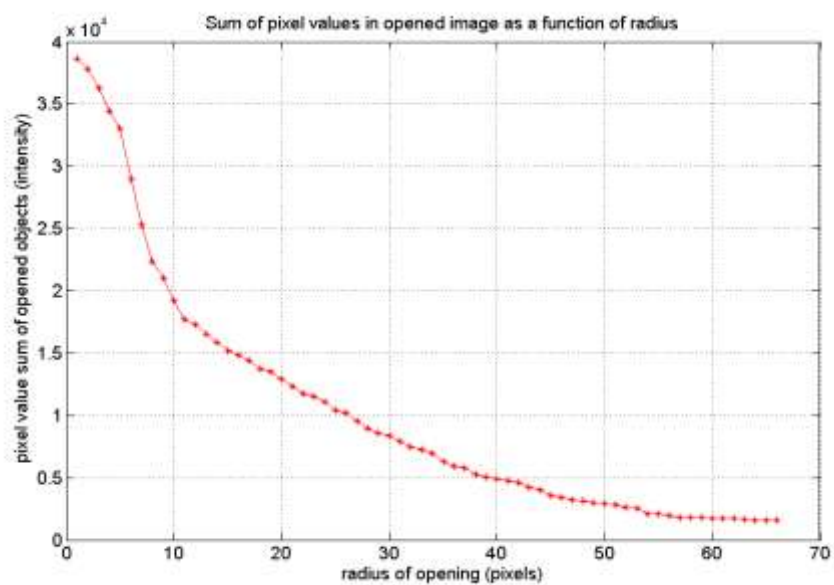


Figure 9: Comparison of forces- Ratio of magnetic to buoyancy forces acting along a diffusion flame, Re=15



**Figure 10:** Soot samples collected at flame tip for a case of no magnetic field (top) and vertically decreasing magnetic field ( $B_{\max}=0.3$  T) (bottom)



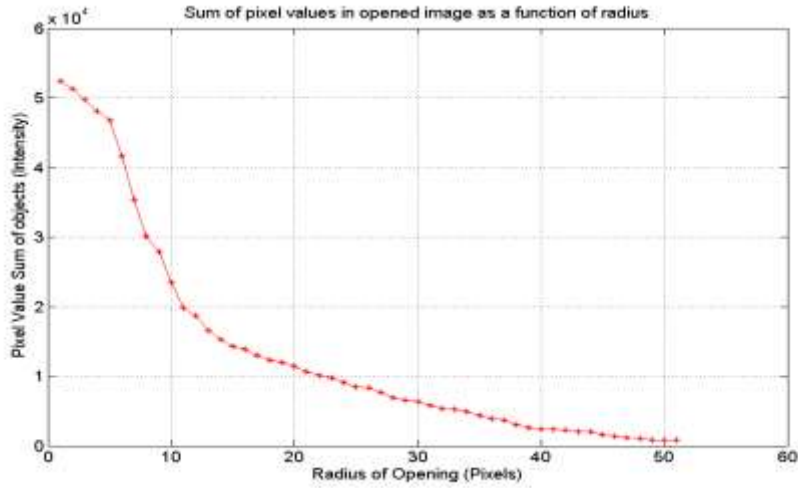


Figure 11: Surface Area Intensity plot for no applied magnetic field (top) and decreasing gradient magnetic field (bottom)

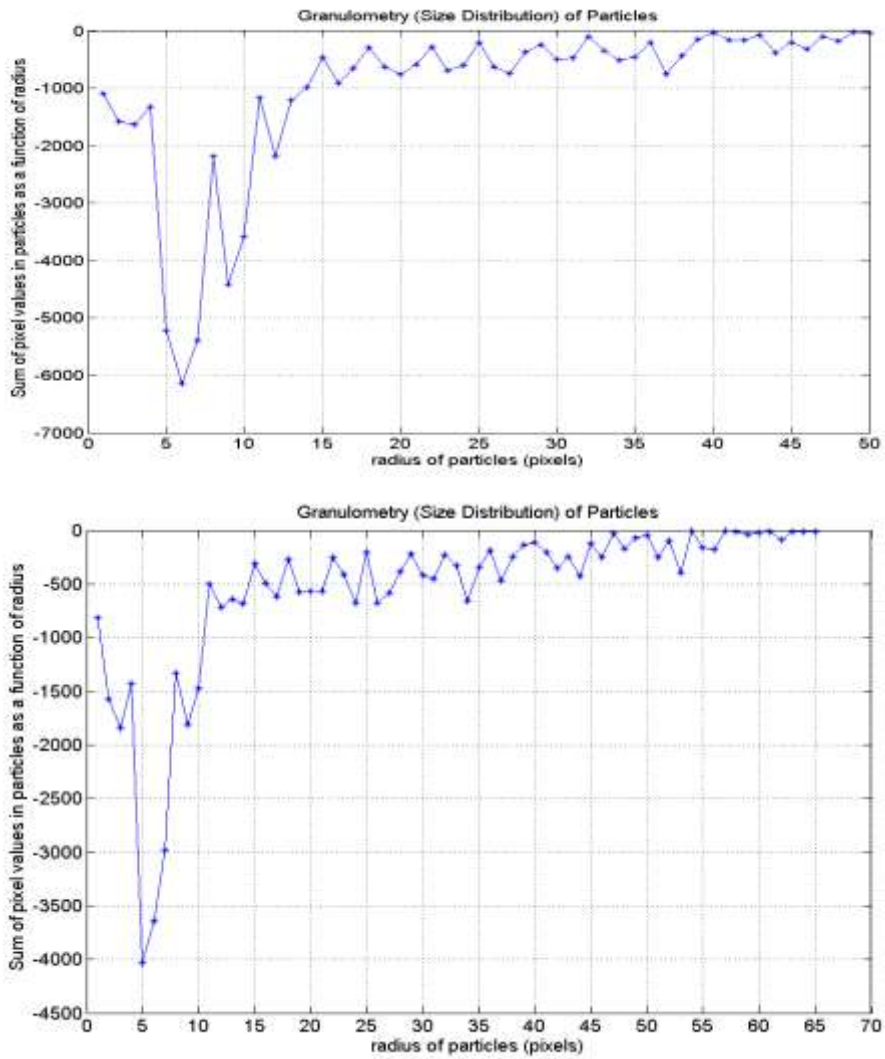
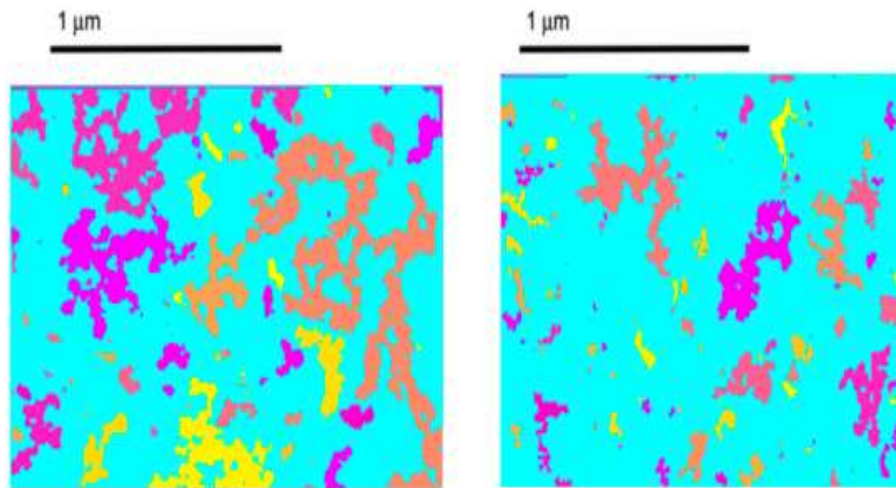
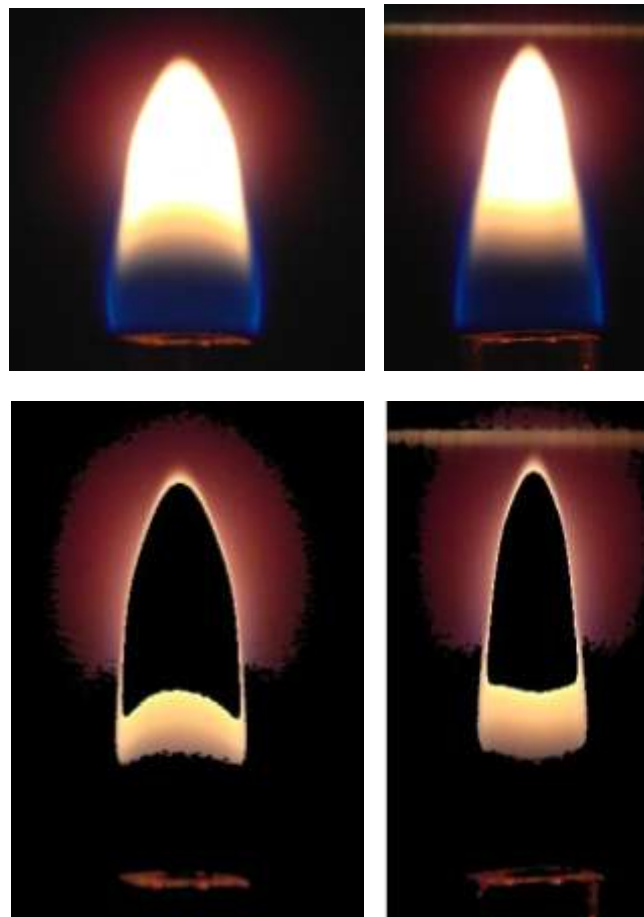


Figure 12: Size distribution for no applied magnetic field (top) decreasing gradient magnetic field (bottom)



**Figure 13:** Color indexed images of continuous objects in soot agglomerates



**Figure 14:** Enhanced flame images for jet exit velocity of 2.5 cm/sec for no magnetic field (left) and spherical magnetic field on diffusion flame (right)

Diego Gonzalez" Effects of Magnetic Fields on Diffusion Flames" Quest Journals Journal of Research in Mechanical Engineering 5.1 (2019): 08-20